

Article

Experimental Study of Damage Evolution in Circular Stirrup-Confined Concrete

Zuohua Li ^{1,2}, Zhihan Peng ^{1,2,*}, Jun Teng ^{1,2,*} and Ying Wang ^{3,*}

¹ School of Civil and Environment Engineering, Shenzhen Graduate School, Harbin Institute of Technology, Shenzhen 518055, China; lizuohua@hit.edu.cn (Z.L.); hayespeng@gmail.com (Z.P.)

² IoT Application Technology Center of NDT, Shenzhen Graduate School, Harbin Institute of Technology, Shenzhen 518055, China

³ Department of Civil and Environmental Engineering, University of Surrey, Guildford GU2 7XH, UK

* Correspondence: tengj@hit.edu.cn (J.T.); ying.wang@surrey.ac.uk (Y.W.);

Tel.: +86-755-26033806 (J.T.); +44-1483-683995 (Y.W.); Fax: +86-755-26033509 (J.T.)

Academic Editor: Jorge de Brito

Received: 27 January 2016; Accepted: 31 March 2016; Published: 8 April 2016

Abstract: This paper presents an experimental study on circular stirrup-confined concrete specimens under uniaxial and monotonic load. The effects of stirrup volume ratio, stirrup yield strength and concrete strength on damage evolution of stirrup-confined concrete were investigated. The experimental results showed that the strength and ductility of concrete are improved by appropriate arrangement of the stirrup confinement. Firstly, the concrete damage evolution can be relatively restrained with the increase of the stirrup volume ratio. Secondly, higher stirrup yield strength usually causes larger confining pressures and slower concrete damage evolution. In contrast, higher concrete strength leads to higher brittleness, which accelerates the concrete damage evolution. A plastic strain expression is obtained through curve fitting, and a damage evolution equation for circular stirrup-confined concrete is proposed by introducing a confinement factor (C) based on the experimental data. The comparison results demonstrate that the proposed damage evolution model can accurately describe the experimental results.

Keywords: concrete; confinement; circular stirrups; damage evolution; experimental study

1. Introduction

In engineering applications, the allocation of reinforcement stirrups is an important measure to improve the mechanical properties of compression members or other structural components under compression because stirrups allocated perpendicularly to the axial compression/maximum principal stress orientation are able to confine the transverse deformation of the core concrete. Stirrup-confined concrete have been studied since 1903, when Considère and Moisseiff [1] first indicated that transverse stirrups improved the deformation capability of axial compression columns. Over the past century, numerous researchers have conducted theoretical and experimental studies on confined concrete including damage related functions and numerical models, *etc.* by using different approaches (Richart *et al.*, 1928 [2]; Kent and Park, 1971 [3]; Sheikh and Uzumeri, 1980 [4]; Mander *et al.*, 1988 [5]; Karabinis and Kiousis, 1994 [6]; Spoelstra and Monti, 1999 [7]; Montoya *et al.*, 2004 [8]; Papanikolaou and Kappos, 2007 [9]; Rousakis *et al.*, 2008 [10]; Karabinis *et al.*, 2008 [11]; Monti and Nisticò, 2008 [12]; Moghaddam *et al.*, 2010 [13]; Jiang and Wu, 2012 [14]; Peter *et al.*, 2013 [15]; Nisticò and Monti, 2013 [16]; Nisticò *et al.*, 2014 [17]; Gambarelli *et al.*, 2014 [18]; Nisticò, 2014 [19]; Wei and Wu, 2014 [20]). These studies confirmed that confinement (steel and/or FRP) improved the strength of reinforced concrete members. Particularly for the high-strength concrete with stirrup confinement, the strength increased much higher than that of unconfined concrete [21]. Not only improving the concrete strength, stirrups can lead to the increase of the

ultimate compressive strain so the ductility is improved as well [5,13]. In order to quantify these effects, various confined concrete stress-strain models have been proposed by numerous researchers (Kent and Park, 1971 [3]; Sheikh and Uzumeri, 1982 [22]; Mander *et al.*, 1988 [23]; Saatcioglu and Razvi, 1992 [24]; Cusson and Paultre, 1995 [25]; Moghaddam *et al.*, 2010 [26]; Samani and Attard, 2012 [27]).

Concrete is a multiphase composite quasi-brittle material, and its damage mechanism is complicated. The cracking process of concrete is different from those of other brittle materials. Research indicated that when maximum principal stress reaches a certain level, a large number of microcracks may exist in concrete, especially at the interface between coarse aggregates and mortar [28,29]. Concrete cracking process, which can be studied at a microscopic or even macroscopic level [30], is a continuous formation and merging of microcracks. Such a process eventually leads to the concentration of multiple microcracks in a very narrow area, and then a visible macrocrack forms, which causes the cross-section stiffness degradation [31,32]. Numerous modern measurement techniques have been applied to the research on concrete damage mechanism at a microscopic level, with reliable results [33–40], but sophisticated equipment is required. Numerical simulation is another option. However, because of the complexity of numerical algorithms and the computational cost, efforts on the simulation of the detailed evolution (growth and coalescence) of each microcrack in stirrup-confined concrete are inefficient. Alternatively, the phenomenological approach at the macroscopic level could be used to describe the effects of microcracks on the damage evolution. Macroscopic phenomenology studies of concrete damage mechanism have obtained excellent achievements, which improved the understanding of concrete damage evolution by measuring the variation of material properties (e.g., elastic modulus and compression strength) [41–45], whereas most of these studies concentrated on unconfined concrete and the research on damage evolution of stirrup-confined concrete has not been systematically conducted yet.

This paper aims to investigate the damage evolution in circular stirrup-confined concrete specimens through experimental study. The tangent module degradation was defined as a damage indicator, and it was subsequently used to obtain damage evolution curves. Furthermore, the effects of stirrup volume ratio, stirrup yield strength and concrete strength on damage evolution of the stirrup-confined concrete are discussed. To describe the effects of various confinement parameters on concrete damage evolution, a damage evolution equation is proposed by introducing a confinement factor (C). The proposed damage evolution equation can represent the experimental results reasonably.

2. Specimen Tests

2.1. Materials

Three groups of concrete with different strengths named as groups C1, C2 and C3 were prepared for concrete specimens. The material compositions of those concrete are listed in Table 1. The compressive strength of 150 mm × 150 mm × 150 mm concrete cubes were measured according to the Chinese Standard GB/T 50081-2002 [46]. The 28-day cubic compressive strength of each group is listed in Table 2. Standard deviations of three test results are 0.66, 0.91 and 1.9, respectively, much lower than the standard requirement [47]. Two groups of stirrups named Y1 and Y2 with different yield strengths were used, with diameters of 6.0 and 6.5 mm, respectively. The diameter of the longitudinal steel bars was 10.0 mm. Tensile tests were performed to measure yield strength and ultimate tensile strength of stirrups and steel bars, and the results are listed in Table 3. The standard deviations of three test results are much lower than the standard requirement.

Table 1. Material compositions of concrete.

Group	C1	C2	C3
Water (kg/m ³)	185	185	195
Cement (kg/m ³)	285	310	410
Gravel (kg/m ³)	1145	1125	1055
Sand (kg/m ³)	785	780	740

Table 2. 28-day cubic compressive strength of concrete (MPa).

Test	Group		
	A	B	C
1	21.2	25.1	38.9
2	22.0	24.8	40.0
3	20.7	26.5	42.6
Average	21.3	25.5	40.5

Table 3. Yield tensile strength (ultimate tensile strength) of stirrups and longitudinal steel bars (MPa).

Test	Y1	Y2	Longitudinal Steel Bar
	<i>d</i> = 6.0 mm	<i>d</i> = 6.5 mm	<i>d</i> = 10.0 mm
1	372 (518)	553 (652)	393 (530)
2	368 (522)	518 (672)	385 (529)
3	370 (520)	538 (669)	390 (532)
Average	370 (520)	536 (664)	389 (530)

2.2. Specimen Design

Thirty standard circular concrete specimens were manufactured with the same dimensions of Φ 150 mm \times 300 mm. Among them, eighteen were stirrup-confined concrete specimens, while the other twelve were unconfined concrete specimens. The variables in the tests were concrete compressive strength, stirrup volume ratio and stirrup yield strength. In this study, the compressive strengths of groups A, B, and C concrete are 21.3, 25.5 and 40.5 MPa, respectively. Based on practical engineering experiences, three stirrup volume ratios were chosen as 0.92%, 1.84% and 2.75%, denoted as S1–S3, respectively. Y1 and Y2 denote stirrup yield strengths are 370 and 536 MPa, respectively. S0Y0 denotes the unconfined concrete. The mechanical and geometrical properties of all specimens are listed in Table 4, where λ_v is stirrup characteristic value [48] and ω_{wd} is mechanical volumetric ratio [49], which are given by:

$$\lambda_v = \frac{\rho_v f_y}{f_{cu}} \quad (1)$$

$$\omega_{wd} = \frac{\text{volume of confining hoops}}{\text{volume of concrete core}} \times \frac{f_y}{f_{cu}} \quad (2)$$

Table 4. Mechanical and geometrical properties of all specimens.

Group	Specimen	f_{cu} (MPa)	<i>d</i> (mm)	<i>s</i> (mm)	ρ_v (%)	f_y (MPa)	λ_v	ω_{wd}	Number of Specimens
C1	C1S0Y0	21.3	–	–	–	–	–	–	4
C1	C1S2Y1	21.3	6.5	70	1.65	370	0.29	0.29	3
C1	C1S2Y2	21.3	6	70	1.65	536	0.42	0.42	3
C2	C2S0Y0	25.5	–	–	–	–	–	–	4
C2	C2S1Y1	25.5	6.5	140	0.82	370	0.12	0.12	3
C2	C2S2Y1	25.5	6.5	70	1.65	370	0.24	0.24	3
C2	C2S3Y1	25.5	6.5	46.7	2.47	370	0.36	0.36	3
C3	C3S0Y0	40.5	–	–	–	–	–	–	4
C3	C3S2Y1	40.5	6.5	70	1.65	370	0.15	0.15	3

For ρ_v is stirrup volume ratio, λ_v and ω_{wd} has the same meaning with different minimum required values. The minimum ω_{wd} is 0.12 for column critical region at the base or 0.08 for column critical region above the base [49]. Accordingly, λ_v have the minimum required values in range of 0.05–0.24 for

columns with different anti-seismic grades, stirrup types and axial compression ratios [48]. It seems that the minimum ω_{wd} is in the middle range of the minimum λ_v . It is suitable and safe for common structural design. The construction drawing of a representative specimen C2S3Y1 with a stirrup spacing of 46.7 mm is shown in Figure 1 as an example.

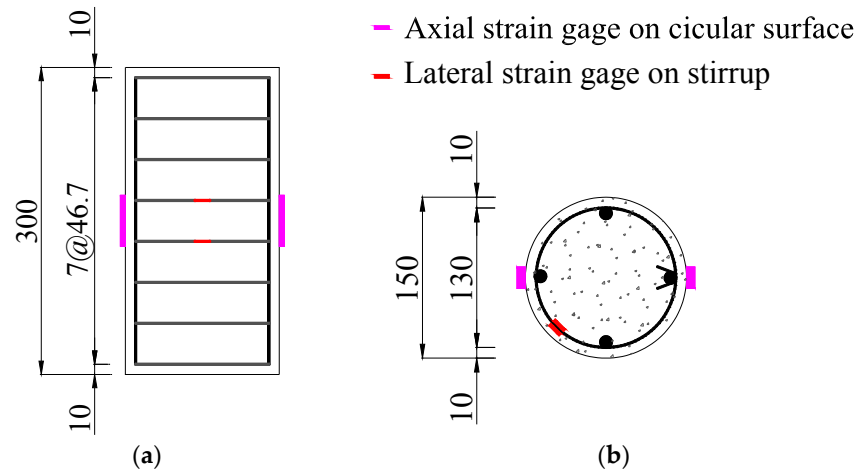


Figure 1. Construction drawing of specimen C2S3Y1 and locations of axial strain gauges and lateral strain gauges: (a) horizontal view; and (b) top view (unit: mm).

2.3. Test Procedure

The loading tests were performed using a 1000 kN MTS electro-hydraulic servo system; the overall view of test setup is shown in Figure 2a. Two 50-mm axial strain gauges were attached on the surface of specimens at mid-height. The axial deformations of specimens were measured by two LVDTs. The locations of axial strain gauges and LVDTs are shown in Figure 2b. The loading of the tests was displacement controlled with a loading rate of $0.4 \times 10^{-4} \text{ s}^{-1}$.

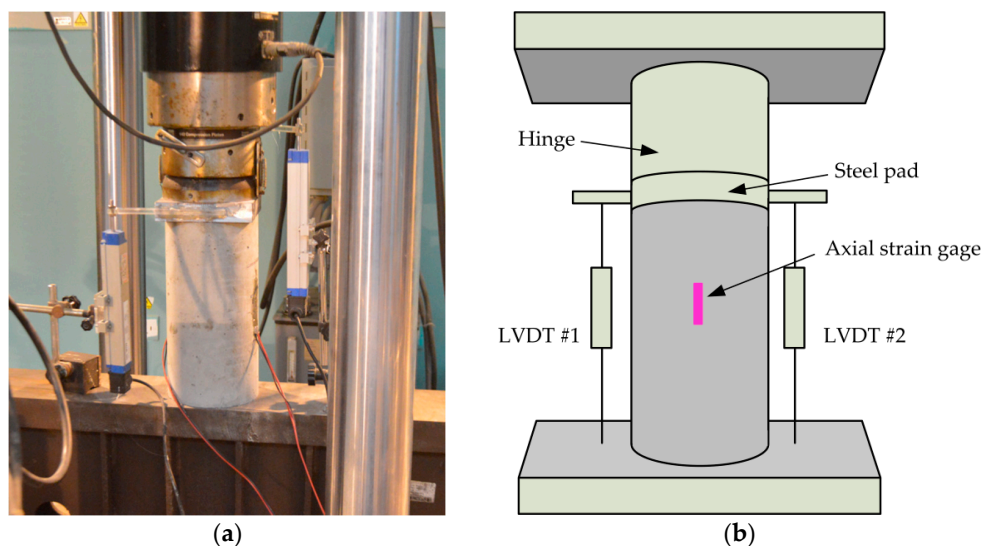


Figure 2. Test setup and instrumentation: (a) test setup; and (b) locations of strain gauges and LVDTs.

In this study, monotonic and cyclic loading compression tests were performed on all the specimens. Prior to the tests, the specimens were pre-loaded to 10% of the estimated peak load and then held for 60 s to eliminate the slackness of test system and avoid the eccentricity of loading by adjusting specimen position until strain gage readings were consistent.

The cyclic loading compression tests were performed on both unconfined and stirrup-confined concrete specimens. A constant strain increment ($\Delta\varepsilon$) was used in each test. Because of the discrepancy in strain between specimens, two loading conditions with different strain increments were selected in the tests. For unconfined concrete, the magnitudes of strain increment ($\Delta\varepsilon$) in two loading conditions were 5.0×10^{-4} and 7.5×10^{-4} , whereas for stirrup-confined concrete specimens, the magnitudes were 1.00×10^{-3} and 1.25×10^{-3} or 0.50×10^{-3} and 1.00×10^{-3} . Loading rate was 4×10^{-5} /s for all specimens.

3. Test Results

3.1. Monotonic Loading Tests

The monotonic stress-strain curves of all specimens are shown in Figure 3. Compared with unconfined concrete specimens, the stirrup-confined concrete specimens had visibly higher stress-strain peaks. Additionally, the ascending curves of stirrup-confined concrete specimens show a linear portion followed by a plateau and the descending curves were considerably broader with greater ductility. The stirrups yielded around the peak stress, at which the confinement effects were greatest.

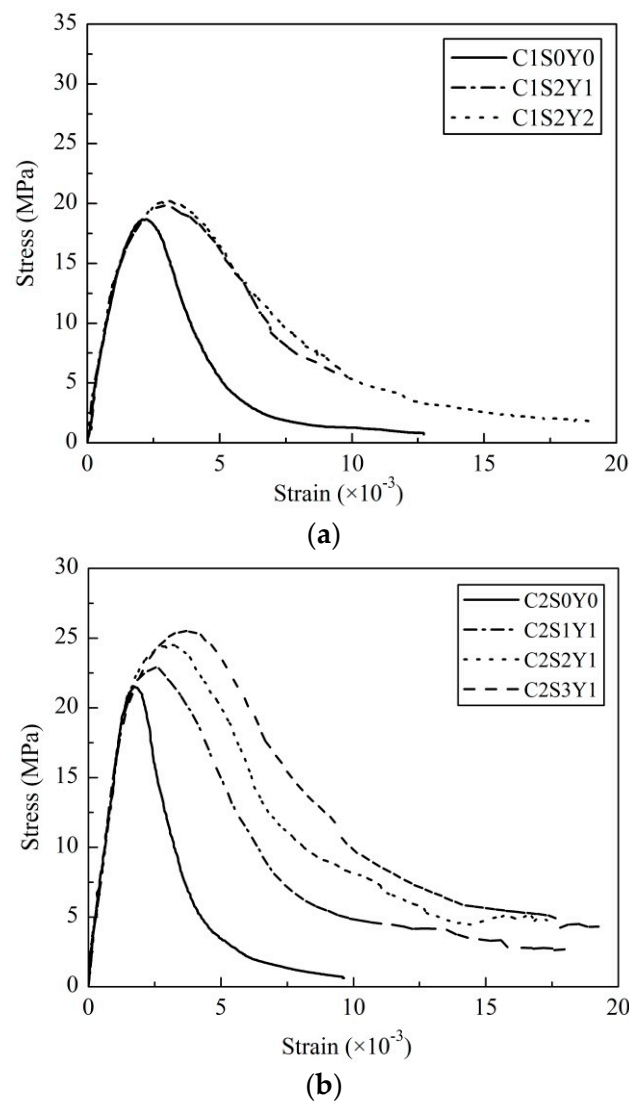


Figure 3. Cont.

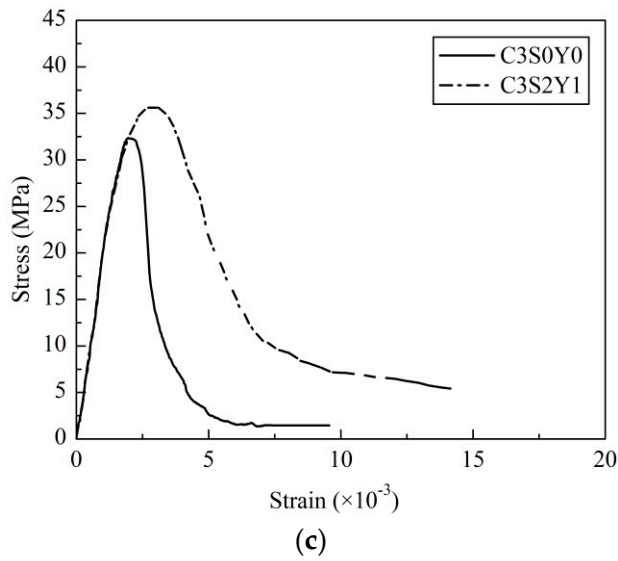


Figure 3. Monotonic stress-strain curves for: (a) Group C1 ($f_{cu} = 21.3$ MPa); (b) Group C2 ($f_{cu} = 25.5$ MPa); and (c) Group C3 ($f_{cu} = 40.5$ MPa).

3.2. Cyclic Loading Tests

Figure 4 shows the stress-strain curves of two typical specimens under cyclic loading. The curves of unconfined concrete specimen C2S0Y0 are shown in Figure 4a,b, and those of stirrup-confined specimen C2S2Y1 are shown in Figure 4c,d. The corresponding monotonic stress-strain curves are also shown in the same figures. The envelope curves of cyclic loading tests present similar behavior with monotonic loading tests.

In the cyclic stress-strain curves, three characteristic behaviors can be observed:

1. When the load reached a certain level, complete unloading always led to plastic deformation. The strain of unloading points increased with the loading/unloading process progressed.
2. The curves showed obvious stiffness degradation during unloading process. With loading cycles increased, the unloading elastic modulus decreased continuously.
3. The stirrup-confined concrete bore more loading/unloading cycles with higher ultimate strain compared with the unconfined concrete when failure occurred.

In this study, two typical cyclic loading curves were selected for discussion. Curves of the remaining 14 specimens showed similar features, shown in Appendix (Figures A1 and A2).

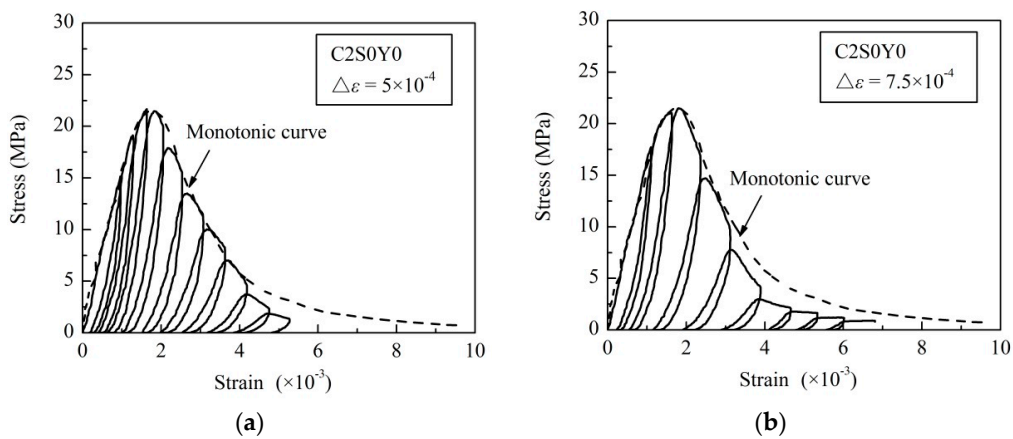


Figure 4. Cont.

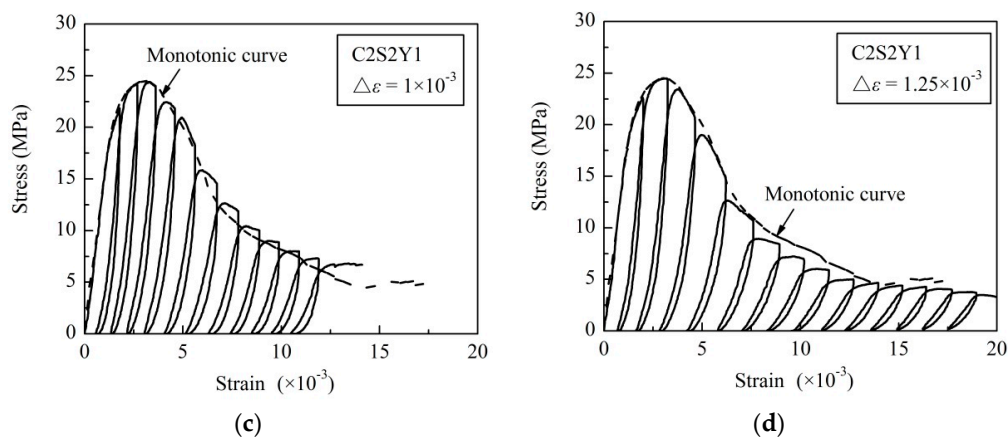


Figure 4. Cyclic stress–strain curves for: (a) unconfined concrete specimen (C2S0Y0) $\Delta\varepsilon = 5.0 \times 10^{-4}$; (b) unconfined concrete specimen (C2S0Y0) $\Delta\varepsilon = 7.5 \times 10^{-4}$; (c) stirrup-confined concrete specimen (C2S2Y1) $\Delta\varepsilon = 1.00 \times 10^{-3}$; and (d) stirrup-confined concrete specimen (C2S2Y1) $\Delta\varepsilon = 1.25 \times 10^{-3}$.

3.3. Failure Modes

Figure 5 shows the failure modes under monotonic loading of typical stirrup-confined concrete specimen C2S3Y1 and unconfined concrete specimen C1S0Y0, respectively. For the stirrup-confined concrete specimen C2S3Y1, the initial longitudinal microcracks were formed parallel to the axial direction. With the increase of load, longitudinal microcracks progressed from both ends toward the center and merged with other longitudinal microcracks. Failure occurred after buckling of the longitudinal steel bars, and was explosive with total loss in load bearing capacity during stirrup relative slips. The stirrups bowed out due to the expansion of core concrete with upper end failure, as shown in Figure 5a. The stirrup slips made anti-buckling detailing failed, causing the longitudinal steel bars buckling. It suggested that the detailing preventing buckling and anchorage failure were important for confined concrete compression performance [50]. In contrast, for unconfined concrete specimen C2S0Y0, independent microcracks progressed, producing a major longitudinal macrocrack through the cross section, as shown in Figure 5b. It showed that load-bearing capacity reduced more rapidly after peak load and that the failure was more sudden and explosive.

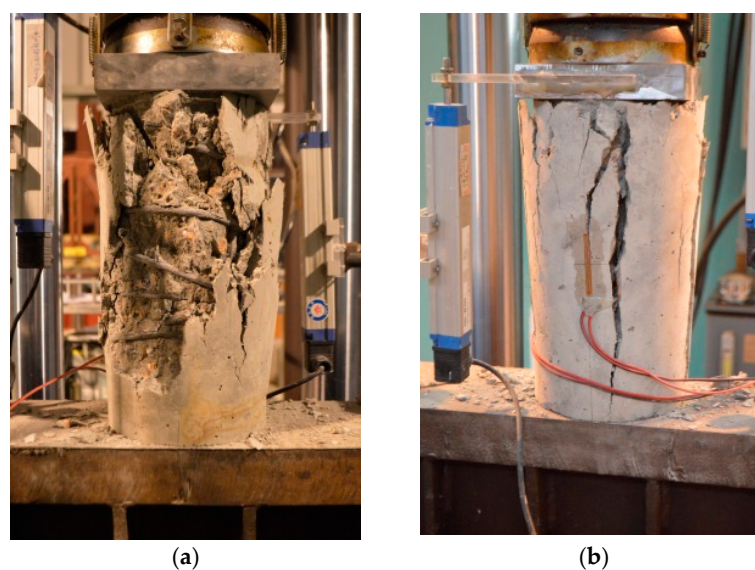


Figure 5. Failure patterns: (a) stirrup-confined concrete specimen (C2S3Y1); and (b) unconfined concrete specimen (C1S0Y0).

4. Analysis and Discussions

4.1. Strength and Ductility of Stirrup-Confined Concrete

The test results for all specimens are listed in Table 5. The average peak compressive strain (ϵ_{c0}) for three groups of unconfined concrete specimens was evaluated as 1.94×10^{-3} , while those of the stirrup-confined concrete (ϵ_{cc}) were in the range of 2.56×10^{-3} – 3.76×10^{-3} . The ultimate compressive strain was defined as the strain when stress softened to 50% peak compressive stress. The average ultimate compressive strain (ϵ_{cu}) of three groups of unconfined concrete was 3.33×10^{-3} , while those of the stirrup-confined concrete (ϵ_{ccu}) were in the range of 5.59×10^{-3} – 8.76×10^{-3} . The peak compressive stress ratios (f_{cc}/f_{c0}) and the corresponding peak compressive strain ratios ($\epsilon_{cc}/\epsilon_{c0}$) between stirrup-confined and unconfined concrete specimens are all greater than 1 for all specimens. The values of f_{cc}/f_{c0} were in range of 1.07–1.19. Compared with the concrete strength improvement, the peak strain showed a more remarkable enhancement; $\epsilon_{cc}/\epsilon_{c0}$ were in the range of 1.43–2.12. In addition, the ultimate compressive strain ratios ($\epsilon_{ccu}/\epsilon_{cu}$) were in the range of 1.70–2.79. It clearly indicated the stirrup confinement improved concrete ductility.

Table 5. Test results.

Group	Specimen	f_{c0} or f_{cc} (MPa)	ϵ_{c0} or ϵ_{cc} (10^{-3})	ϵ_{cu} or ϵ_{ccu} (10^{-3})	f_{cc}/f_{c0}	$\epsilon_{cc}/\epsilon_{c0}$	$\epsilon_{ccu}/\epsilon_{cu}$
C1	C1S0Y0	18.69	2.09	4.02	–	–	–
C1	C1S2Y1	19.92	2.98	6.85	1.07	1.43	1.70
C1	C1S2Y2	20.23	3.1	7.27	1.08	1.48	1.81
C2	C2S0Y0	21.5	1.77	3.14	–	–	–
C2	C2S1Y1	22.92	2.56	5.92	1.07	1.45	1.89
C2	C2S2Y1	24.57	3.09	6.88	1.14	1.75	2.19
C2	C2S3Y1	25.59	3.76	8.76	1.19	2.12	2.79
C3	C3S0Y0	32.35	1.97	2.83	–	–	–
C3	C3S2Y1	35.8	2.87	5.59	1.11	1.46	1.98

Table 6 compares the prediction performances using typical confined concrete models with the values involving peak compressive stress ratio (f_{cc}/f_{c0}) and corresponding peak compressive strain ratio ($\epsilon_{cc}/\epsilon_{c0}$). In the table, for Kent and Park model [3], the underestimation of $\epsilon_{cc}/\epsilon_{c0}$ may be caused by using the same expression to estimate enhancements in both strength and strain, which is relatively approximate. The model proposed by Saatcioglu and Razvi [24] appears to give the estimable prediction of circular stirrup-confined concrete compared with the test results. For the theoretical model of Mander *et al.* [23], the test results show a difference with the prediction, which may be caused by the lower confinement effect because the specimen size limits the confinement densification detailing at the specimen end.

Table 6. Existing models to predict f_{cc}/f_{c0} and $\epsilon_{cc}/\epsilon_{c0}$.

Model	Peak Strength	Peak Strain	f_{cc}/f_{c0}	$\epsilon_{cc}/\epsilon_{c0}$
Kent and Park [3]	$\frac{f_{cc}}{f_{c0}} = 1 + \frac{\rho_s f_y}{f_{c0}}$	$\frac{\epsilon_{cc}}{\epsilon_{c0}} = 1 + \frac{\rho_s f_y}{f_{c0}}$	1.14–1.47	1.14–1.47
Mander <i>et al.</i> [23]	$\frac{f_{cc}}{f_{c0}} = 2.254 \sqrt{1 + 7.94 \frac{f_{le}}{f_{c0}} - 2 \frac{f_{le}}{f_{c0}} - 1.254}$	$\frac{\epsilon_{cc}}{\epsilon_{c0}} = 1 + 5 \left(\frac{f_{cc}}{f_{c0}} - 1 \right)$	1.11–1.84	1.54–5.21
Saatcioglu and Razvi [24]	$\frac{f_{cc}}{f_{c0}} = 1 + 6.7 \frac{f_{le}^{0.83}}{f_{c0}}$	$\frac{\epsilon_{cc}}{\epsilon_{c0}} = 1 + 5 \frac{k_1 f_{le}}{f_{c0}}$	1.12–1.3	1.61–2.51
Present tests	–	–	1.07–1.19	1.43–2.12

4.2. Damage Evolution of Stirrup-Confined Concrete

4.2.1. Plastic Strain

The cyclic loading tests in this study showed that after a certain load limit was reached, the complete unloading of each loading cycle generated irreversible residual deformation, known as plastic deformation [51,52]. The strain of unloading point increased with the loading/unloading cycle continued, leading to higher levels of deformation, as shown in Figure 4.

By applying a quadratic polynomial expression to the ϵ_p - ϵ relationship experimentally obtained, two functions were obtained for unconfined and stirrup-confined concrete, respectively. For simplicity, a unified function was proposed for both stirrup-confined and unconfined concrete specimens.

$$\epsilon_p = \begin{cases} 0 & \forall \epsilon \leq \epsilon_{ce} \\ c(\epsilon - \epsilon_{ce})^2 + d(\epsilon - \epsilon_{ce}) & \forall \epsilon > \epsilon_{ce} \end{cases} \quad (3)$$

For comparison, a linear function is fitted, and the results are plotted together with the test data shown in Figure 6. The plastic strain curve of confined concrete shows more elastoplastic behavior. However, for unconfined concrete, it shows that the curve of linear fitting is an upper bound in intermediate strain range of 2.0×10^{-3} – 5.0×10^{-3} , and quadratic polynomial fitting is close to an average curve in that range. With parameters $c = 6.283$ and $d = 0.831$, the proposed function of stirrup-confined concrete shows good correlation with the experimental data with $R^2 = 0.997$, as shown in Figure 6a. Similarly, the parameters of unconfined concrete were obtained and a good correlation of $R^2 = 0.988$ is observed, as shown in Figure 6b.

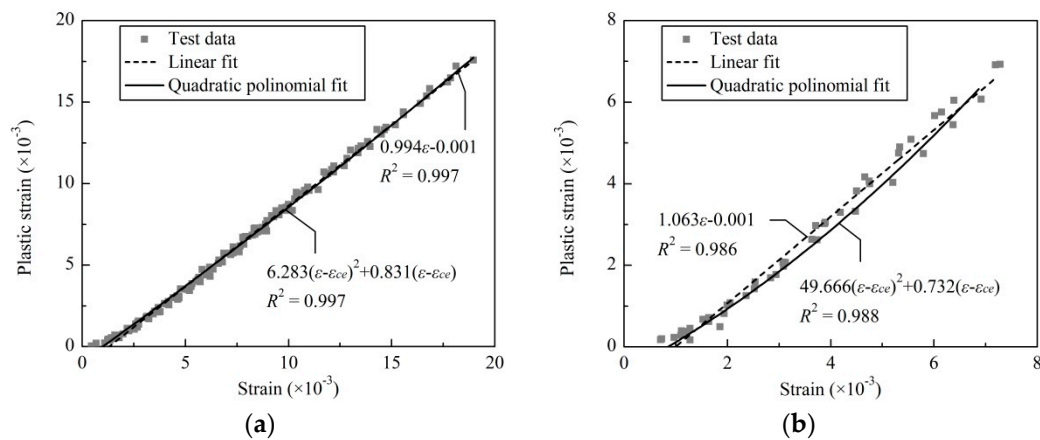


Figure 6. Proposed function for the ϵ_p - ϵ relationship: (a) stirrup-confined concrete; and (b) unconfined concrete.

4.2.2. Effects on Concrete Damage Evolution

The cyclic loading tests clarify that the concrete stiffness degrades because of the development of microcracks with the increase of plastic strain. In order to describe this phenomenon, a damage indicator D was defined to represent the evolution of concrete damage by Lemaitre [53]. According to this concept, the damage indicator D can be calculated by means of Equation (4), where E_0 is initial elastic modulus and E_u is unloading secant stiffness of the line connecting present unloading point to next loading point in the loading cycles.

$$D = 1 - E_u/E_0 \quad (4)$$

The effects of the stirrup volume ratio, stirrup yield strength and concrete strength on concrete damage evolution were investigated by comparing the test results, which are illustrated in Figure 7.

Figure 7a shows the effect of stirrup yield strength on the damage evolution of specimens with identical concrete strength and stirrup volume ratio, 21.3 MPa and 1.65%, respectively. It can be observed that the damage evolution of specimens with 536 MPa stirrup yield strength proceeded more slowly than those of specimens with 370 MPa stirrup yield strength. It demonstrates that the stirrup confinement effect is affected by stirrup yield strength to some extent. Higher stirrup yield strength leads to a higher confining pressure while inhibiting concrete damage evolution.

Figure 7b shows the effect of stirrup volume ratio on the damage evolution of specimens with identical concrete and strengths stirrup yield strengths, 25.5 and 370 MPa, respectively. For unconfined concrete specimens, damage emerged at $\varepsilon = 2.0 \times 10^{-3}$ and the curves increased sharply, suggesting rapid damage evolution. With stirrups allocated, damage emerged at strain in the range of 2.0×10^{-3} – 4.0×10^{-3} , indicating that the damage evolution was delayed significantly. As compared with unconfined concrete, the damage evolution curve was gradual and longer. It is also observed in Figure 7b that the slopes of the curves gradually decreased, and that the ultimate compressive strain increased, as the stirrup volume ratio increased from 0.82% to 2.47%. It clearly demonstrates that when the stirrup volume ratio increased, the concrete damage evolution was restrained.

Figure 7c shows the effect of concrete strength on the damage evolution of specimens with identical stirrup volume ratios and yield strengths, 1.65% and 370 MPa, respectively. The high-strength concrete damage evolved more rapidly than low-strength concrete. The reason is that high-strength concrete exhibited limited transverse deformation under axial compression relatively, and a lower passive confinement effect was observed. In addition, internal microcracks generation and merging processes were more rapid in high-strength concrete than those in normal concrete, which leads to a faster damage evolution.

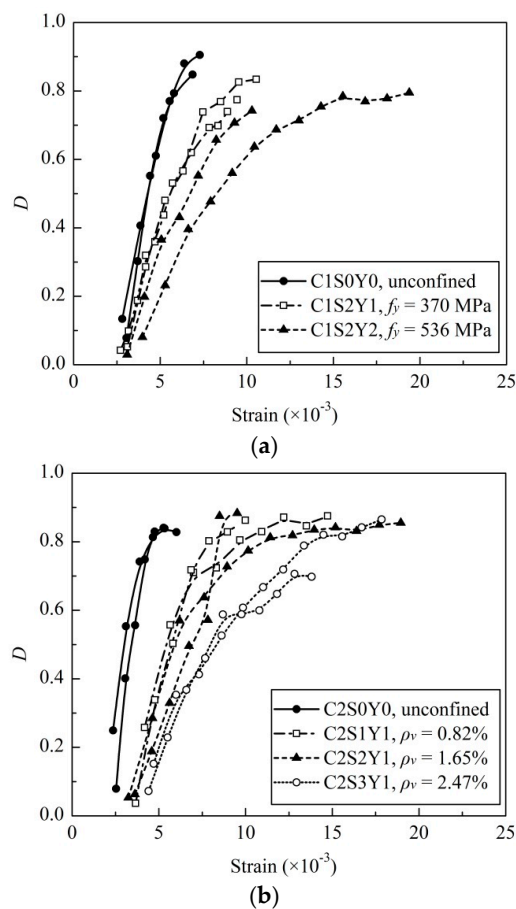


Figure 7. Cont.

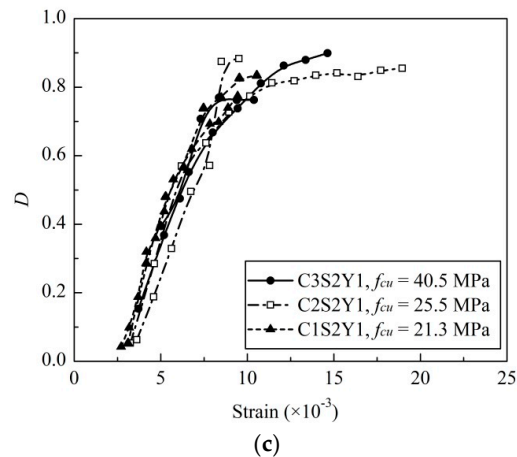


Figure 7. (a) Effect of stirrup volume ratio on damage evolution; (b) effect of stirrup yield strength on damage evolution; and (c) effect of concrete strength on damage evolution.

4.3. Proposed Damage Evolution Equation

Figure 8 shows the damage evolution curve of a typical stirrup-confined concrete specimen (C1S2Y1, blue line) with stress–strain curve of monotonic compression (black line) superimposed. The test results revealed that the shapes of stress–strain curves of stirrup-confined concrete specimens were different from those of the unconfined concrete specimens. The former curves were broader, with an interval point located on the gradually declining branch, which was less steep than the latter curves ($d^2\sigma/d\varepsilon^2 = 0$ at the interval point). Based on the strain at interval point ε_{in} , the plastic phase could be divided into two stages: plastic stage 1 and plastic stage 2. The damage evolution also presented distinct features in the different states:

1. In the elastic stage (Curve OA in Figure 8), no damage appeared, meant D was very small (close or equal to zero).
2. Plastic stage 1 included the ascending branch before peak stress and the declining branch after peak stress up to interval point. In the ascending branch, microcracks formed quickly, which resulted in rapid damage evolution, although with a small amount of damage (Curve AB in Figure 8). After peak stress, the crack merging processes progressed further, and damage accumulated during this stage. However, damage began to stabilize because of stirrup confinement effect (Curve BC in Figure 8).
3. In plastic stage 2, few new microcracks were generated, and damage increased very slowly while loading increased continuously until failure occurred (Curve CD in Figure 8).

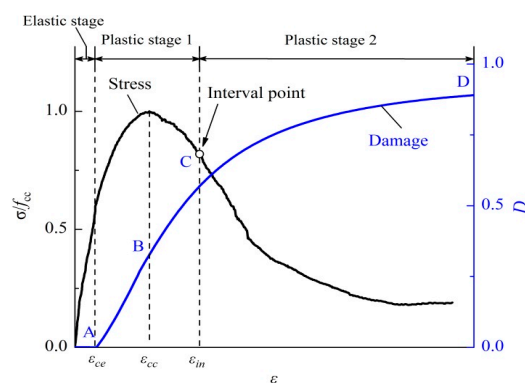


Figure 8. Characteristics of the damage evolution curve showing the different stages (Elastic, Plastic 1, and Plastic 2) related to the stress (left axis) and damage (right axis).

The evolution of damage indicator of stirrup-confined concrete (D_{cc}) is modified from D_c by multiplying a confinement factor (C) as follows

$$D_{cc} = \begin{cases} 0 & \forall \varepsilon \leq \varepsilon_{ce} \\ C \times D_c & \forall \varepsilon > \varepsilon_{ce} \end{cases} \quad (5)$$

where D_c is the damage indicator of unconfined concrete defined by Li and Li [54], which is given by

$$D_c = 1 - \frac{1}{1 + \left(\frac{Y_c - a_c}{b_c}\right)^{l_c}} \quad (6)$$

where Y_c is damage energy release rate (Li and Li [54]), which is given by

$$Y_c = \left(1 + k_c \frac{\varepsilon_p}{\varepsilon}\right) \times \frac{E_0 \varepsilon_{ce}^2}{2} \quad (7)$$

In Equations (6) and (7), a_c , b_c , l_c and k_c are parameters of unconfined concrete (Li and Li [54]) that need be calibrated with experimental data and their values are summarized in Table 7.

Table 7. The parameter of a_c , b_c , l_c and k_c used to calculate damage.

Group	a_c	b_c	l_c	k_c
C1	0.0113	-0.191	1.0	-2.719
C2	0.0110	-0.432	1.0	-7.071
C3	0.0227	-1.579	1.0	-1.579

Considering the different features of damage evolution before and after the interval point mentioned above, the expression of confinement factor (C) is given by

$$C = \begin{cases} \exp [m (-3.150 - n \times \sqrt{\varepsilon} \times \ln(\varepsilon))] & \forall \varepsilon \leq \varepsilon_{in} \\ \arctan (A_m (\varepsilon - \varepsilon_{in})) \times 2(1 - C_{in})/\pi + C_{in} & \forall \varepsilon > \varepsilon_{in} \end{cases} \quad (8)$$

where C_{in} is confinement factor corresponding to $\varepsilon_{in} \times C_{in} = 0.5$ is suggested through the calibration with test data. The parameters m , n , and A_m in Equation (8), which are obtained by the regression analysis of experimental results, are given by:

$$m = 0.06319 f_{cc}^{1.1} \times (1.296 - \lambda_v^{0.7})^2 \quad (9)$$

$$n = 0.53494 f_{cc}^{0.15} \times f_y^{0.15} (5 - 1.79 \lambda_v^{0.2}) \quad (10)$$

$$A_m = \exp(5.3 + 0.1 \times f_{cc}^{0.4} / \lambda_v^{0.6}) \quad (11)$$

The comparisons of proposed damage evolution with experimental results of the three stirrup-confined concrete specimen groups C1, C2 and C3 are shown in Figure 9. The damage began to increase from zero at a strain range of 2.0×10^{-3} – 4.0×10^{-3} , displaying the same plastic deformation developments as those of the experimental data. The damage increased significantly before eventually stabilizing at $D_{cc} = 0.8$ – 0.9 , corresponding to the ultimate strain. In most cases, the proposed damage evolution curve accurately simulates the experiment results. It can be used to develop plastic damage models of stirrup-confined concrete.

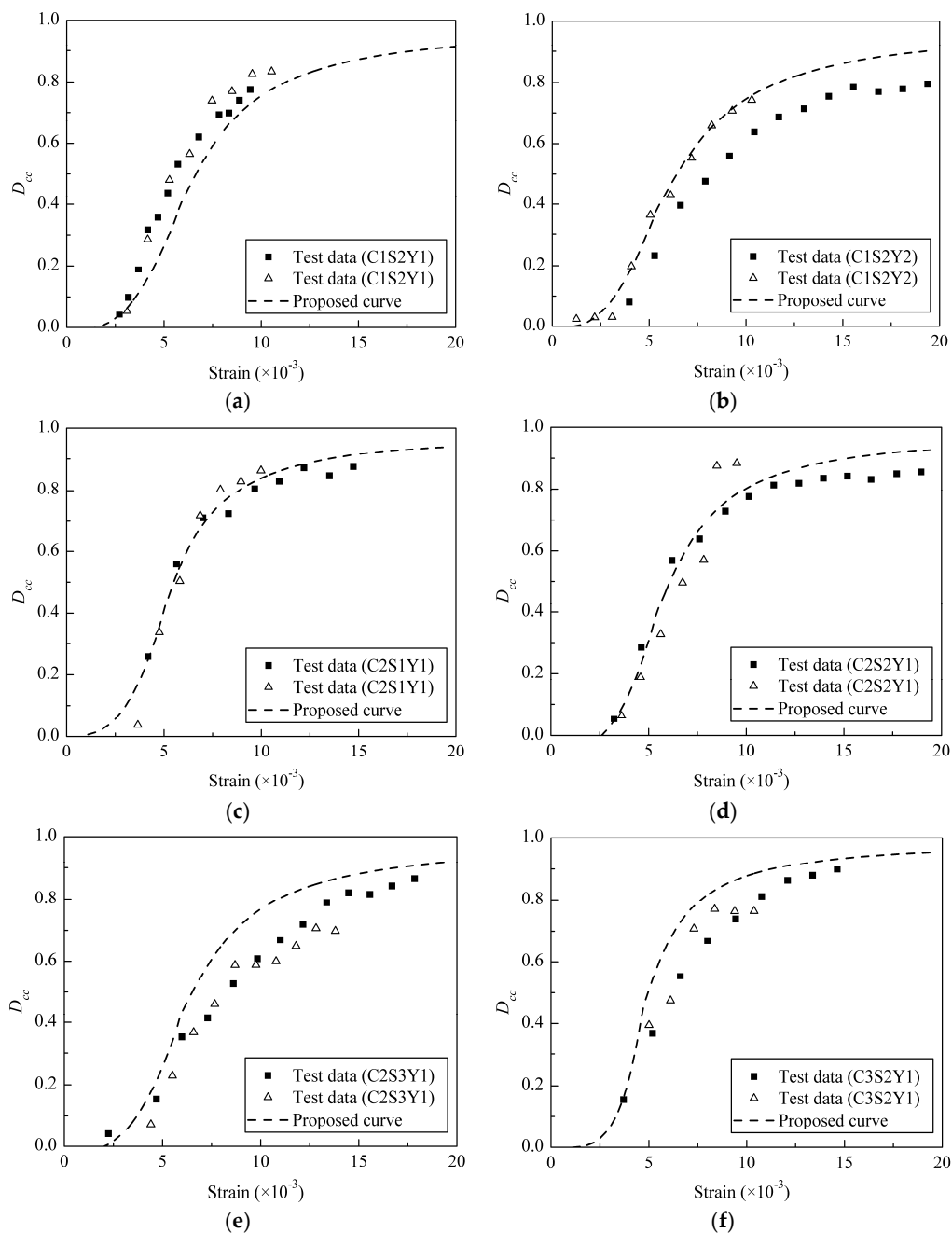


Figure 9. Comparisons of the proposed D_{cc} to the experimental results of specimens: (a) C1S2Y1; (b) C1S2Y2; (c) C2S1Y1; (d) C2S2Y1; (e) C2S3Y1; and (f) C3S2Y1.

5. Conclusions

A study of damage evolution of circular stirrup-confined concrete specimens under monotonic and cyclic compression loadings was presented. The effects of stirrup volume ratio, stirrup yield strength and concrete strength on stress-strain curves and damage evolution of stirrup-confined concrete were investigated. Based on experimental results, expressions for plastic deformation and damage evolution were proposed. The following conclusions can be drawn from this study:

- Strength and ductility of reinforced concrete can be improved by stirrup confinement effect. The ratio f_{cc}/f_{c0} was introduced to describe the concrete strength improvement, which ranged from

1.07 to 1.19; additionally, the peak strain and ultimate strain displayed remarkable enhancements, as $\varepsilon_{cc}/\varepsilon_{c0}$ and $\varepsilon_{ccu}/\varepsilon_{cu}$ were in the range of 1.43–2.12 and 1.70–2.79, respectively.

- The stirrup-confined concrete specimens showed clear transverse expansion instead of brittle failure, and the stirrups bowed out when failure occurred. The stirrups with lower stirrup volume ratios show limited confinement effect. At higher stirrup volume ratios, the stirrups provide higher confinement effect. Thus, the stirrup volume ratios play an important role in transverse confining of concrete.
- Confining pressure from stirrups reduces microcrack formation and restrained the damage evolution of concrete. As stirrup volume ratio increases, the stirrups provide a stronger transverse confining pressure, further restraining the damage evolution of concrete. Higher stirrup yield strength can generate a larger confining pressure, which would inhibit damage evolution. Due to the brittleness of high-strength concrete, growth and merging of microcracks proceed rapidly, causing the acceleration of damage evolution.
- Based on experimental results, a plastic strain expression was proposed, and a confinement factor (C) was introduced to the proposed damage evolution equation, to describe the effects of various confinement parameters on concrete damage evolution. The established damage evolution model can well represent the whole damage evolution process in circular stirrup-confined concrete. Because of less confinement parameters involved, the model can be conveniently applied to evaluate the plastic damage behavior of circular stirrup-confined concrete with reasonable accuracy.
- Evidently, more test results are needed to fully validate the proposed model. In addition, the size effect of specimen on damage evolution model was not considered in the present study. As such, the proposed damage evolution model for circular stirrup-confined concrete can be refined in future research works.

Acknowledgments: The authors would like to thank the Major International (Sino-US) Joint Research Project of the National Natural Science Foundation of China (Grant No. 51261120374), the National Natural Science Foundation of China (Grant No. 51378007), and Shenzhen Technology Innovation Program—Technology Development Projects (Grant No. CXZZ20140904154839135).

Author Contributions: Zuohua Li and Jun Teng proposed the topic of this study and monitored the whole research project. Zhihan Peng performed the experiments, test data analysis and initial draft writing of the manuscript. Ying Wang participated in the discussions of test results and led a thorough revision of the manuscript. All authors read and approved the final manuscript.

Conflicts of Interest: The authors declare no conflict of interest.

Abbreviations

The following abbreviations are used in this manuscript:

IoT	Internet of Things
NDT	Non Destructive Testing
LVDT	Linear Variable Differential Transformer

List of Symbols

d	Stirrup diameter
s	Stirrup spacing
ρ_v	Stirrup volume ratio
λ_v	Stirrup characteristic value
f_y	Stirrup yield strength
f_{cu}	Cubic compressive strength of the concrete
F_0	Ultimate load of the unconfined concrete
F_c	Ultimate load of the stirrup-confined concrete

E_0	Elastic modulus of the unconfined concrete
E_c	Elastic modulus of the confined concrete
E_u	Secant stiffness of the line connecting present unloading point to next loading point
f_{c0}	Peak compressive stress of the unconfined concrete
f_{cc}	Peak compressive stress of the stirrup-confined concrete
ε	Strain
$\Delta\varepsilon$	Strain increment
ε_{c0}	Peak compressive strain corresponding to f_{c0}
ε_{cc}	Peak compressive strain corresponding to f_{cc}
ε_{cu}	Ultimate compressive strain of the unconfined concrete
ε_{ccu}	Ultimate compressive strain of the stirrup-confined concrete
ε_{ce}	Elastic compressive limit strain of the stirrup-confined concrete
ε_p	Plastic strain
ε_{in}	Plastic strain at the interval point
D_c	Damage indicator of unconfined concrete
D_{cc}	Damage indicator of stirrup-confined concrete
C	Confinement factor
C_{in}	Confinement factor corresponding to ε_{in}
Y_c	Damage energy release rate function

Appendix

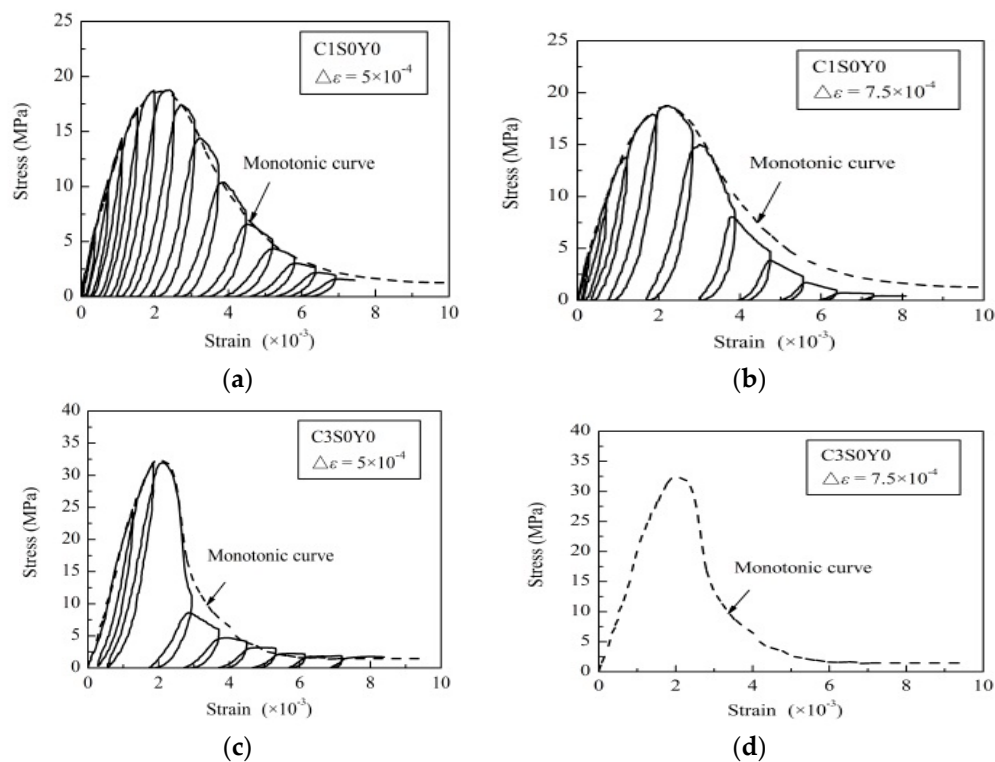


Figure A1. Cyclic stress–strain curves of unconfined concrete specimen: (a) C1S0Y0, $\Delta\varepsilon = 5.0 \times 10^{-4}$; (b) C1S0Y0, $\Delta\varepsilon = 7.5 \times 10^{-4}$; (c) C3S0Y0, $\Delta\varepsilon = 5.0 \times 10^{-4}$; and (d) C3S0Y0, $\Delta\varepsilon = 7.5 \times 10^{-4}$.

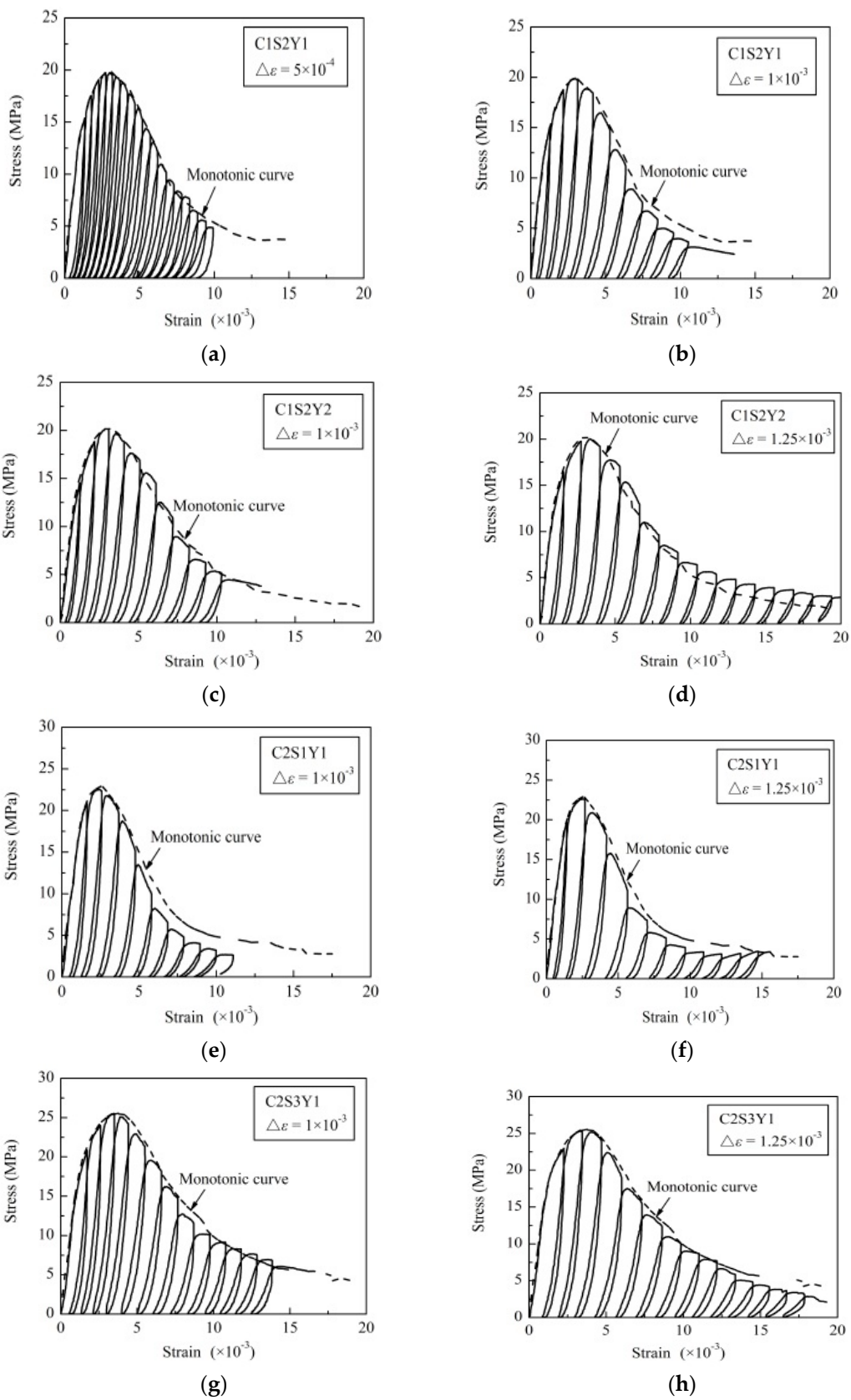


Figure A2. Cont.

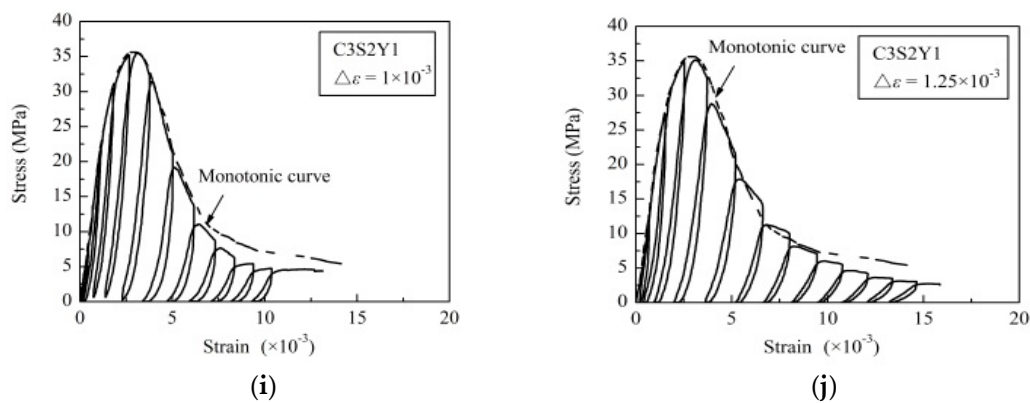


Figure A2. Cyclic stress-strain curves of stirrup-confined concrete specimen: (a) C1S2Y1, $\Delta\epsilon = 5.00 \times 10^{-4}$; (b) C1S2Y1, $\Delta\epsilon = 1.00 \times 10^{-3}$; (c) C1S2Y2, $\Delta\epsilon = 1.00 \times 10^{-3}$; (d) C1S2Y2, $\Delta\epsilon = 1.25 \times 10^{-3}$; (e) C2S1Y1, $\Delta\epsilon = 1.00 \times 10^{-3}$; (f) C2S1Y1, $\Delta\epsilon = 1.25 \times 10^{-3}$; (g) C2S3Y1, $\Delta\epsilon = 1.00 \times 10^{-3}$; (h) C2S3Y1, $\Delta\epsilon = 1.25 \times 10^{-3}$; (i) C3S2Y1, $\Delta\epsilon = 1.00 \times 10^{-3}$; and (j) C3S2Y1, $\Delta\epsilon = 1.25 \times 10^{-3}$.

References

1. Considère, A.; Moisseiff, L.S. *Experimental Research on Reinforced Concrete*; McGraw Publishing: New York, NY, USA, 1906.
2. Richart, F.E.; Brandtzaeg, A.; Brown, R.L. *A Study of the Failure of Concrete under Combined Compressive Stresses*; Bulletin No. 185; Engineering Experimental Station, University of Illinois: Urbana, IL, USA, 1928.
3. Kent, D.C.; Park, R. Flexural members with confined concrete. *J. Struct. Div. ASCE* **1971**, *97*, 1969–1990.
4. Sheikh, S.A.; Uzumeri, S.M. Strength and ductility of tied concrete columns. *J. Struct. Div. ASCE* **1980**, *106*, 1079–1102.
5. Mander, J.B.; Priestley, M.J.N.; Park, R. Observed Stress-Strain Behavior of Confined Concrete. *J. Struct. Eng.* **1988**, *114*, 1827–1849. [[CrossRef](#)]
6. Karabinis, A.I.; Kioussis, P.D. Effects of confinement on concrete columns: Plasticity approach. *J. Struct. Eng. ASCE* **1994**, *120*, 2747–2767. [[CrossRef](#)]
7. Spoelstra, M.R.; Monti, G. FRP-confined concrete model. *J. Compos. Constr.* **1999**, *3*, 143–150. [[CrossRef](#)]
8. Montoya, E.; Vecchio, F.J.; Sheikh, S.A. Numerical evaluation of the behaviour of steel- and FRP-confined concrete columns using compression field modeling. *Eng. Struct.* **2004**, *26*, 1535–1545. [[CrossRef](#)]
9. Papanikolaou, V.K.; Kappos, A.J. Confinement-sensitive plasticity constitutive model for concrete in triaxial compression. *Int. J. Solids Struct.* **2007**, *44*, 7021–7048. [[CrossRef](#)]
10. Rousakis, T.C.; Karabinis, A.I.; Kioussis, P.D.; Tepfers, R. Analytical modelling of Plastic Behaviour of Uniformly FRP Confined Concrete Members. *Compos. B Eng.* **2008**, *39*, 1104–1113. [[CrossRef](#)]
11. Karabinis, A.I.; Rousakis, T.C.; Manolitsi, G. 3D Finite Element Analysis of Substandard Columns Strengthened by Fiber Reinforced Polymer Sheets. *J. Compos. Constr.* **2008**, *12*, 531–540. [[CrossRef](#)]
12. Monti, G.; Nisticò, N. Square and rectangular concrete columns confined by CFRP: Experimental and numerical investigation. *Mech. Compos. Mater.* **2008**, *44*, 289–308. [[CrossRef](#)]
13. Moghaddam, H.; Samadi, M.; Pilakoutas, K.; Mohebbi, S. Axial compressive behavior of concrete actively confined by metal strips; part A: Experimental study. *Mater. Struct.* **2010**, *43*, 1369–1381. [[CrossRef](#)]
14. Jiang, J.F.; Wu, Y.F. Identification of material parameters for Drucker-Prager plasticity model for FRP confined circular concrete columns. *Int. J. Solids Struct.* **2012**, *49*, 445–456. [[CrossRef](#)]
15. Peter, G.; Dimitrios, X.; Ulrika, N.; Rasmus, R.; Kent, G. CDPM2: A damage-plasticity approach to modelling the failure of concrete. *Int. J. Solids Struct.* **2013**, *15*, 3805–3816.
16. Nisticò, N.; Monti, G. RC square sections confined by FRP: Analytical prediction of peak strength. *Compos. B Eng.* **2013**, *45*, 127–137. [[CrossRef](#)]
17. Nisticò, N.; Pallini, F.; Rousakis, T.; Wu, Y.F.; Karabinis, A. Peak strength and ultimate strain prediction for FRP confined square and circular concrete sections. *Compos. B Eng.* **2014**, *67*, 543–554. [[CrossRef](#)]

18. Gambarelli, S.; Nisticò, N.; Ožbolt, J. Numerical analysis of compressed concrete columns confined with CFRP: Microplane-based approach. *Compos. B Eng.* **2014**, *67*, 303–312. [[CrossRef](#)]
19. Nisticò, N. RC square sections confined by FRP: A numerical procedure for predicting stress-strain relationships. *Compos. B Eng.* **2014**, *59*, 238–247. [[CrossRef](#)]
20. Wei, Y.; Wu, Y.F. Compression behavior of concrete columns confined by high strength steel wire. *Constr. Build. Mater.* **2014**, *54*, 443–453. [[CrossRef](#)]
21. Cusson, D.; Paultre, P. High-strength concrete columns confined by rectangular ties. *J. Struct. Eng.* **1994**, *120*, 783–804. [[CrossRef](#)]
22. Sheikh, S.A.; Uzumeri, S.M. Analytical model for concrete confinement in tied columns. *J. Struct. Div. ASCE* **1982**, *108*, 2703–2722.
23. Mander, J.B.; Priestley, M.J.N.; Park, R. Theoretical stress-strain model for confined concrete columns. *J. Struct. Eng.* **1988**, *114*, 1804–1826. [[CrossRef](#)]
24. Saatcioglu, M.; Razvi, S.R. Strength and ductility of confined concrete. *J. Struct. Eng.* **1992**, *118*, 1590–1607. [[CrossRef](#)]
25. Cusson, D.; Paultre, P. Stress-strain model for confined high-strength concrete. *J. Struct. Eng.* **1995**, *12*, 468–477. [[CrossRef](#)]
26. Moghaddam, H.; Samadi, M.; Pilakoutas, K. Compressive behavior of concrete actively confined by metal strips, part B: Analysis. *Mater. Struct.* **2010**, *43*, 1383–1396. [[CrossRef](#)]
27. Samani, A.K.; Attard, M.M. A stress-strain model for uniaxial and confined concrete under compression. *Eng. Struct.* **2012**, *41*, 335–349. [[CrossRef](#)]
28. Chen, W.F. *Constitutive Equations for Engineering Materials. Volume 2: Plasticity and Modeling*; Elsevier: New York, NY, USA, 1994.
29. Chen, W.F. *Plasticity in Reinforced Concrete*; McGraw-Hill: New York, NY, USA, 1982.
30. Krajcinovic, D. Damage mechanics: Accomplishments, trends and needs. *Int. J. Solids Struct.* **2000**, *37*, 267–277. [[CrossRef](#)]
31. Shaochun, M.; Nan, J. Seismic Experimental Study on New-Type Composite Exterior Wallboard with Integrated Structural Function and Insulation. *Materials* **2015**, *8*, 3732–3753.
32. Løland, K.E. Continuous damage model for load-response estimation of concrete. *Cem. Concr. Res.* **1980**, *10*, 395–402. [[CrossRef](#)]
33. Bang, Y.L.; Su-Tae, K.; Hae-Bum, Y.; Yun, Y.K. Improved Sectional Image Analysis Technique for Evaluating Fiber Orientations in Fiber-Reinforced Cement-Based Materials. *Materials* **2016**, *9*, 42. [[CrossRef](#)]
34. Ramamoorthy, S.K.; Kane, Y.; Turner, J.A. Ultrasound diffusion for crack depth determination in concrete. *J. Acoust. Soc. Am.* **2004**, *115*, 523–529. [[CrossRef](#)] [[PubMed](#)]
35. Francisco, J.B.; Oscar, G.; Emilio, Z.; Pedro, G. Multifunctional Cement Composites Strain and Damage Sensors Applied on Reinforced Concrete (RC) Structural Elements. *Materials* **2013**, *6*, 841–855.
36. Abdelrahman, M.; ElBatanouny, M.K.; Ziehl, P.H. Acoustic emission based damage assessment method for prestressed concrete structures: Modified index of damage. *Eng. Struct.* **2014**, *60*, 258–264. [[CrossRef](#)]
37. Omar, A.A.; Mohd, M.A.B.A.; Kamarudin, H.; Khairul, N.I.; Mohammed, B.I. Mechanical and Microstructural Evaluations of Lightweight Aggregate Geopolymer Concrete before and after Exposed to Elevated Temperatures. *Materials* **2013**, *6*, 4450–4461.
38. Shahiron, S.; Rhys, P.; Norazura, M.B.; Karen, M.H. Damage classification in reinforced concrete beam by acoustic emission signal analysis. *Constr. Build. Mater.* **2013**, *45*, 78–86.
39. Yoseok, J.; Jaeha, L.; WooSeok, K. Modeling and Measurement of Sustained Loading and Temperature-Dependent Deformation of Carbon Fiber-Reinforced Polymer Bonded to Concrete. *Materials* **2015**, *8*, 435–450.
40. Anugonda, P.; Wiehn, J.S.; Turner, J.A. Diffusion of ultrasound in concrete. *Ultrasonics* **2001**, *39*, 429–435. [[CrossRef](#)]
41. Jun, L.; Feng, X.; Biqin, D.; Hongyan, M.; Dong, P. Study on Surface Permeability of Concrete under Immersion. *Materials* **2014**, *7*, 876–886.
42. Cook, D.J.; Chindaprasirt, P. Influence of loading history upon the tensile properties of concrete. *Mag. Concr. Res.* **1981**, *33*, 154–160. [[CrossRef](#)]
43. Shiyun, X.; Hongnan, L.; Paulo, J.M.M. Influence of strain rates and loading histories on the compressive damage behaviour of concrete. *Mag. Concr. Res.* **2011**, *63*, 915–926.

44. Poinard, C.; Malecot, Y.; Daudeville, L. Damage of concrete in a very high stress state: Experimental investigation. *Mater. Struct.* **2010**, *43*, 15–29. [[CrossRef](#)]
45. Gettu, R.; Aguado, A.; Oliveira, M.F. Damage in high-strength concrete due to monotonic and cyclic compression—A study based on splitting tensile strength. *ACI Mater. J.* **1996**, *93*, 519–523.
46. *China Standard GB/T 50081-2002: Standard for Test Method of Mechanical Properties on Ordinary Concrete*; China Architecture & Building Press: Beijing, China, 2003.
47. *China Standard GB/T 50107-2010: Standard for Evaluation of Concrete Compressive Strength*; China Architecture & Building Press: Beijing, China, 2010.
48. *China Standard GB/T 50011-2010: Standard for Seismic Design of Buildings*; China Architecture & Building Press: Beijing, China, 2010.
49. *European Standard Eurocode 8: Design of Structures for Earthquake Resistance Part 1: General Rules, Seismic Actions and Rules for Buildings*; European Committee for Standardization: Brussels, Belgium, 2004.
50. Rousakis, T.C.; Karabinis, A.I. Adequately FRP confined reinforced concrete columns under axial compressive monotonic or cyclic loading. *Mater. Struct.* **2012**, *45*, 957–975. [[CrossRef](#)]
51. Bazant, Z.P.; Kim, S. Plastic-fracturing theory for concrete. *J. Eng. Mech. Div. ASCE* **1979**, *105*, 407–428.
52. Sinha, B.P.; Gerstle, K.H.; Tulin, L.G. Stress-strain relations for concrete under cyclic loading. *J. ACI* **1964**, *61*, 195–212.
53. Lemaitre, J. A continuous damage mechanics model for ductile fracture. *J. Eng. Mater. Technol.* **1985**, *107*, 83–89. [[CrossRef](#)]
54. Li, Z.H.; Li, A.; Teng, J. A plastic-damage uniaxial compression constitutive of concrete. *China Civ. Eng. J.* **2012**, *45*, 182–186.



© 2016 by the authors; licensee MDPI, Basel, Switzerland. This article is an open access article distributed under the terms and conditions of the Creative Commons Attribution (CC-BY) license (<http://creativecommons.org/licenses/by/4.0/>).